# Electrophonon resonance in $Al_xGa_{1-x}As$-GaAs quasi-two-dimensional quantum wells

K. Král*
*Department of Physics, National Cheng Kung University, Tainan, Taiwan, Republic of China*
(Received 27 August 1993; revised manuscript received 1 June 1994)

The electrophonon resonance, based on the long-wavelength optical-phonon population detectable by the Raman-scattering technique and on the hot-electron cooling rate, is studied theoretically with the aim of obtaining the separate contributions of the confined and interface modes to the resonance pattern. Two models of optical phonons are applied to a semiconductor $Al_xGa_{1-x}As$-GaAs quantum well with the square shape of the potential profile: the bulk phonons of the GaAs and the dielectric continuum model of the optical phonons in a quantum well. The control of the onset of the resonant intersubband optical-phonon scattering is assumed to be provided by means of either varying the quantum-well width or the applied homogeneous electric field normal to the interfaces. The electrophonon resonance based on the detection of the long-wavelength optical-phonon population is shown to give a strongly modulated resonance pattern for both the confined modes and the interface modes. The intensities of the resonance patterns due to the confined and the interface phonons appear to be comparable with each other for a broad range of well widths.

## I. INTRODUCTION

A basic role in the understanding of transport properties of semiconductor quantum wells is played by the interaction between charge carriers and lattice vibrations. The interaction of the conduction electrons with the optical phonons is of fundamental importance in bulk semiconductors like GaAs and in low-dimensional semiconductor structures[1,2] at temperatures above 50 K. In low-dimensional structures, in which the electronic motion is confined at least in one dimension, an electron-energy subband structure emerges. Physical properties of such a quantum-well structure may then appear to be quite sensitive to the ratio between the intersubband energy separations and the energies of the optical phonons, especially in the vicinity of the onset of the resonant intersubband optical-phonon scattering (RISOPS).[3] The electron-energy levels can be brought into resonance with the optical-phonon energy upon varying an external parameter. Various parameters suitable for the tuning of the onset of RISOPS were considered. Besides varying the quantum-well dimensions, such as quantum-well width, the static electric field normal to the interfaces of the quasi-two-dimensional (Q2D) quantum well (QW) also has been considered for the tuning of the onset of the resonance.[4,5] In the case when the electric field is used to control the onset of RISOPS, the effect is called electrophonon resonance,[5] although this term is sometimes used even in the case when the onset of RISOPS is controlled simply by varying the quantum-well width for the sake of simplicity of the calculations.[5]

From the point of view of obtaining information about the electron-subband structure and on the energies of optical phonons, it may be desirable to understand the resonant intersubband optical-phonon-scattering effect as manifested in various physical quantities available in experiment. In this respect, the high field electronic transport was studied by Briggs and Leburton[3] using the Monte Carlo technique of semiclassical simulation of electronic motion in quantum wires, under the presence of the resonant intersubband optical-phonon scattering. Peeters, Devreese, and Xu[4,5] studied the electron mobility and electron-scattering rate in Q2D parabolic, square, and triangular quantum wells. The quantum-well width dependence of the hot-electron cooling rate has recently been shown theoretically to display distinct resonant features in $Al_xGa_{1-x}As$-GaAs Q2D quantum wells with a square-shaped potential profile.[6]

Using simple arguments, it becomes readily obvious that under a situation at which RISOPS occurs, namely, when the energy separation of two electronic subbands becomes very close to the optical-phonon energy (resonance condition), the momentum of the optical phonons emitted or absorbed in the course of the corresponding electron-phonon scattering events is nearly zero. The hot-electron cooling rate, calculated without taking the electronic screening into account, displays clearly sharp maxima at such well widths, at which the resonance condition is fulfilled.[6] For this reason the generation of long-wavelength optical phonons can be expected to play an important role in the electrophonon resonance effect.

The question alone of the generation of long-wavelength optical phonons has not been studied in sufficient detail as yet, although this question has been addressed recently in a somewhat different context, namely in connection with the experimental observation of the Raman-scattering signal due to the long-wavelength optical phonons in very thin semiconductor quantum wells.[7-9] In these papers the observation of the nonequilibrium long-wavelength (LW) optical-phonon population in the very thin quantum wells has been ascribed to the influence of the excitonic state in GaAs. Also in these papers, the influence of the interface roughness[10] and the lattice defects have been suggested to be a possible source of the presence of the long-wavelength population in the Raman-scattering experimental data.

0163-1829/94/50(11)/7640(15)/$06.00  

In addition to this, the hot-acoustic-phonon fusion[11,12] and also the collision broadening effect[13,14] have recently been considered as a source of the LW optical-phonon generation. The recent numerical calculation of hot phonon generation in Q2D quantum wells, under the conditions when RISOPS is in effect, has revealed that the optical phonons can be intensively generated in the LW area of the lateral component of the wave vector of the optical phonons.[15] The Raman-scattering detection technique could be a very suitable tool for the study of the resonant intersubband optical-phonon scattering in Q2D quantum wells. It is well known that in the backscattering configuration of the Raman experiment, used for the detection of the population of the hot-optical phonons, only the phonons with a quite small ($<0.07\times10^8$ m$^{-1}$) lateral component of the phonon wave vector can be detected,[2,8,9] because of the total-reflectance angle restrictions. It is, however, this particular region of the phonon wave vector, in which hot phonons are expected to be strongly generated[15] in Q2D quantum wells, when the resonance condition is fulfilled.

Such physical quantities as electronic mobility, the electron-scattering rate, and the hot-electron cooling rate are integral quantities with respect to the generation rate of the distribution function of the optical phonons. This is why in corresponding experiments the resonance features, which are due to the onset of the fulfilment of the resonance condition, can be expected to make only a relatively small contribution to a background, which is due to the dissipative processes of a nonresonant character. The direct measurement of the LW optical-phonon population, as represented by the Raman-scattering technique, could thus provide a convenient means for the study of the electrophonon resonance.

One possible interest when studying the electrophonon resonance may be the suitability of the given detection technique to distinguish between the lattice-vibrational bulk, or confined, modes on one hand, and the interface modes on the other. It may therefore be desirable to test from this point of view the electrophonon resonance effect in the case of the hot-electron cooling, as representative of a technique based on the detection of an integral quantity, in the above-given sense, and the electrophonon resonance based on direct detection of the long-wavelength optical-phonon population.

In this paper the electrophonon resonance is studied for the hot-electron cooling rate and for long-wavelength optical-phonon generation. Two mechanisms are considered to control the onset of the resonant intersubband optical-phonon scattering, varying either the quantum-well width or the applied electric field. The calculations will be restricted to the simple case of an $Al_xGa_{1-x}As$-GaAs quantum well with the square shape of the well-potential profile. The electron-phonon scattering will be treated within the Born approximation, neglecting, e.g., many-body effects such as the collision broadening of the electronic energies. The influence of holes in the valence bands will be neglected. The electronic screening will be treated at the level of approximation of the Debye-Hückel formula. Separate contributions of both the bulk or confined modes, and of the interface modes to the resonance pattern of the LW population of the optical phonons will be determined. The physical models of the electronic structure of the quantum well and the optical lattice vibrations are outlined in Sec. II. The generation rates of the optical phonons, and the hot-electron cooling rate, are derived in Sec. III. In Sec. IV the numerical results are presented and discussed.

## II. THE FORMULATION OF THE MODEL

The system of charge carriers is confined to electrons in the conduction-band states. It is assumed that the electrons move in a Q2D quantum well, the potential of which has a square profile in the direction normal ($z$ axis) to the quantum-well interfaces, with the effective mass $m$ of the $\Gamma$ valley of the conduction band of the bulk GaAs inside the well. For the sake of simplicity it is assumed that the potential barriers of the well, placed at the planes $z=\pm d/2$ ($d$ is the well width), are infinitely high. The orbital part of the wave function of a noninteracting electron is

$$\psi_{n,\mathbf{k}}(\mathbf{r})=L^{-1}\exp(i\mathbf{k}\mathbf{r}_{\parallel})\phi_n(z)\ , \tag{1}$$

where $\phi_n(z)$ is the wave function of the motion in the $n$th subband in the direction normal to the interfaces,

$$\phi_n(z)=\left[\frac{2}{d}\right]^{1/2}\sin\left[\frac{\pi n}{d}\left[z+\frac{d}{2}\right]\right]\ , \tag{2}$$

in the interval of $z\in[-(d/2),(d/2)]$, $L^3=V$, $V$ being the volume of the sample. Here $\mathbf{k}$ is the electronic wave vector parallel to the $xy$ plane, and $\mathbf{r}=\{\mathbf{r}_{\parallel},z\}$. The electronic energies corresponding to $\psi_{n,\mathbf{k}}(\mathbf{r})$ are

$$\epsilon_n(\mathbf{k})=E_n+\frac{h^2|\mathbf{k}|^2}{2m}\ , \tag{3}$$

where $E_n=(\hbar^2\pi^2n^2/2md^2)$, $n=1,2,\ldots$, are the energies of the stationary states $\phi_n(z)$. Let us remark that the choice of $d$, as the parameter controlling the onset of RISOPS, allows one to take advantage of the quantum-well symmetry which remains unchanged upon varying this control parameter. This allows for a deeper insight into the role of the individual vibrational modes in the transport processes considered.

The Hamiltonian of the noninteracting electrons is

$$H_e=\sum_{n,\mathbf{k},\sigma}\epsilon_n(\mathbf{k})c^{+}_{n,\mathbf{k},\sigma}c_{n,\mathbf{k},\sigma}\ , \tag{4}$$

where $c^{+}_{n,\mathbf{k},\sigma}$ is the particle operator of an electron in the orbital state (1) and with the spin projection $\sigma$.

Confining the electronic temperatures to $T_e>50$ K, the electrons are supposed to interact only with the optical phonons. The lowest value of the quantum-well width, of the type presently considered at which RISOPS can be observed, is about 200 Å (1 Å$=10^{-10}$ m).[6] At this value of $d$ the interface phonons,[16–18] are usually not very important,[19] and their contribution to the hot electron cooling rate appears to be quite small. This means that to a certain extent the use of a model of the lattice vibrations, which ignores the existence of the interface phonon modes, can be a good approximation.[20] In particular, the vibrational modes of the quantum-well system can be ap-

proximated by the bulk longitudinal-optical (LO)-phonon modes of GaAs in the sample volume $V$. Let us note that there can be some semiconductor structures, in which, though they are Q2D structures, their deviation from the homogeneous three-dimensional bulk is not so large as to cause a mixing of the bulk longitudinal and transverse optical-phonon branches and to form interface modes. The δ-doped quantum wells in GaAs (Refs. 21 and 22) can serve as an example of such a case. In these structures the approximation of the QW lattice vibrations by the LO phonons of GaAs can be expected to be a good approximation. Although the bulk-phonon model does not provide an electrophonon effect with the interface modes, the bulk-phonon approximation will be considered here, in addition to the dielectric continuum model of the quantum-well optical lattice vibrations.

The two optical-phonon models will now be specified as follows. Assuming that the energy of the LO phonons does not depend on the phonon wave vector $\mathbf{Q}$, the Hamiltonian of the unperturbed bulk LO phonons is

$$H_{f1}=\hbar\omega_0\sum_{\mathbf{q},s} b^{+}_{\mathbf{q},s}b_{\mathbf{q},s} \ , \tag{5}$$

where we write the full three-dimensional phonon wave vector $\mathbf{Q}$ as $\mathbf{Q}=(\mathbf{q},s)$, where the two-dimensional vector $\mathbf{q}$ is the projection of $\mathbf{Q}$ onto the $xy$ plane (lateral component), while $s$ is the projection of $\mathbf{Q}$ on the $z$ axis (normal component).

In the representation of the wave functions $\psi_{n,\mathbf{k}}(\mathbf{r})$ given by Eq. (1), the Fröhlich coupling[23] $H_{i1}$ of the electrons and the bulk LO phonons is

$$H_{i1}=\sum_{n,n',\mathbf{k},\mathbf{q},s,\sigma} A_{\mathbf{q},s}(b_{\mathbf{q},s}-b^{+}_{-\mathbf{q},-s})I_{n,n'}(s)c^{+}_{n,\mathbf{k},\sigma}c_{n',\mathbf{k}-\mathbf{q},\sigma} \ , \tag{6}$$

where $b_{\mathbf{q},s}$ is the annihilation operator of the phonon in the state $(\mathbf{q},s)$. The coupling constant $A_{\mathbf{q},s}$ is

$$A_{\mathbf{q},s}=-ie\left[\frac{\hbar\omega_0}{2\varepsilon_0 V}\right]^{1/2}(\kappa_\infty^{-1}-\kappa_0^{-1})^{1/2}\frac{f_q}{Q} \ , \tag{7}$$

where $Q=|\mathbf{Q}|$ and $q=|\mathbf{q}|$. In the last equation we introduce, in an *ad hoc* way, the screening function $f_q$,[24–26] which corresponds to the static and long-wavelength limit of the random-phase approximation (RPA) formula, namely,

$$f_q=\frac{q}{q+PH(q)} \ , \tag{8}$$

where $P=e^2n_P/(2\varepsilon_0\kappa_\infty k_B T_e)$ and

$$H(q)=\int_{-d/2}^{d/2}dz_1\int_{-d/2}^{d/2}dz_2\rho(z_1)\rho(z_2)\exp(-q|z_1-z_2|) \ , \tag{9}$$

$$\rho(z)=|\phi_1(z)|^2 \ .$$

For the purpose of a simple determination of the screening function, we assume all electrons to reside in the lowest electronic subband with $n=1$. In the above given formulas $n_P$ is the areal electronic density, $e>0$ is electronic charge, $\varepsilon_0$ is the permittivity of the free space, $\kappa_\infty$ and $\kappa_0$ are, respectively, the high- and low-frequency dielectric constants (of GaAs in the case of the present bulk model), $k_B$ is the Boltzmann constant, and $T_e$ is the electronic temperature. In (6), $I_{n,n'}(s)$ is a form factor:

$$I_{n,n'}(s)=\int_{-d/2}^{d/2}\phi_n^*(z)e^{isz}\phi_{n'}(z)dz \ . \tag{10}$$

The theory of the optical lattice vibrations of Q2D semiconductor quantum wells has been developed along two main ways, which differ in their complexity. An account of these theories can be found, for example, in Ref. 27. In the microscopic versions of the theory,[28] the motion of the individual atoms of the lattice is simulated. In the macroscopic versions the envelope function of the atomic displacements is calculated.[16,29–32]

In the present paper the dielectric continuum model of the optical phonons in the formulation of Wendler and Pechstedt[16,31] is used. From the crystal lattice point of view, the quantum well presently considered corresponds to the $Al_{0.25}Ga_{0.75}As$-GaAs structure. The classification of the phonon modes is as follows: The phonon modes, which are confined to the GaAs material, are enumerated by the integer $m, m=1,2,\ldots$. Correspondingly, the wavelength of the modulation of the lattice polarization due to these modes, in the direction normal to the interfaces, is $\lambda=2d/m$. Consistent with the assumption of infinitely high barriers of the electronic quantum well, the electrons do not interact with the confined modes of the potential barriers of $Al_xGa_{1-x}As$ in the present model. There are four interface modes in the heterostructure considered. Because of the symmetry with the mirror plane at $z=0$, these modes are either symmetrical ($S$) or antisymmetrical ($A$), according to the $z$-reflection symmetry of that component of the lattice polarization, which is parallel to the interfaces. The interface modes can be classified by the pair $(\mu\nu)$ of indexes, with $\mu=A$ or $S$, and with $\nu=+$ or $-$. In the present case it appears[31] that the modes with $\nu=+$ have energies close to the energies of LO and TO (transverse optical) modes of $Al_{0.25}Ga_{0.75}As$ ($Al_xGa_{1-x}As$ modes), while the modes with $\nu=-$ have energies close to the optical-phonon energies of the bulk GaAs (GaAs modes).

Alternatively, the interface modes can be identified unambiguously due to their energies, so that, numbering the interface modes by the pair index $(\mu\nu)$, the interface phonon frequencies are[31]

$$\Omega_{\mu\nu}(\mathbf{q})=\frac{\varepsilon_1^\mu(\omega_{L1}^2+\omega_{T2}^2)+\varepsilon_2^\mu(\omega_{L2}^2+\omega_{T1}^2)\pm\sqrt{D_\mu}}{2(\varepsilon_1^\mu+\varepsilon_2^\mu)} \ , \tag{11}$$

where

$$D_\mu=[\varepsilon_1^\mu(\omega_{L1}^2+\omega_{T2}^2)+\varepsilon_2^\mu(\omega_{L2}^2+\omega_{T1}^2)]^2 -4(\varepsilon_1^\mu+\varepsilon_2^\mu)(\varepsilon_1^\mu\omega_{L1}^2\omega_{T2}^2+\varepsilon_2^\mu\omega_{L2}^2\omega_{T1}^2) \ . \tag{12}$$

Here

$$\varepsilon_1^S=\kappa_{\infty 1}(1-\gamma) \ , \quad \varepsilon_2^S=\kappa_{\infty 2}(1+\gamma) \ , \quad \varepsilon_1^A=\kappa_{\infty 1}(1+\gamma) \ , \quad \varepsilon_2^A=\kappa_{\infty 2}(1-\gamma) \ , \quad \gamma=e^{-qd} \ , \tag{13}$$

where $\kappa_{\infty j}$, $j=1$, and 2, are high-frequency dielectric constants of GaAs and $Al_xGa_{1-x}As$, respectively, while

$\omega_{L_j}$ and $\omega_{T_j}$ are the respective bulk frequencies of longitudinal and transverse modes.

The Hamiltonian of the free phonons of the quantum well is

$$H_{f2}=\sum_{i,\mathbf{q}}\hbar\Omega_i(\mathbf{q})a_i^{+}(\mathbf{q})a_i(\mathbf{q}) , \tag{14}$$

in which the index $i$ runs through all of the branches of the confined and interface phonons of QW, and $\mathbf{q}$ is the two-dimensional wave vector in the $xy$ plane. The operator $a_i^{+}(\mathbf{q})$ is the creation operator of the QW phonon in branch $i$, with the wave vector $\mathbf{q}$. The confined and interface modes are coupled to the electrons electrostatically, via their lattice polarization field.[16] The interaction operator $H_{i2}$ of the electrons with the phonons of the QW in the dielectric continuum model is

$$H_{i2}=\sum_{j,n,n',\mathbf{q},\mathbf{k},\sigma}\gamma_j^{n,n'}(\mathbf{q})[a_j(\mathbf{q})+a_j^{+}(-\mathbf{q})]c^{+}_{n,\mathbf{k}+\mathbf{q},\sigma}c_{n',\mathbf{k},\sigma} . \tag{15}$$

The coupling constant $\gamma_j^{n,n'}(\mathbf{q})$ is

$$\gamma_j^{n,n'}(\mathbf{q})=\int_{-d/2}^{d/2}dz\,\phi_n^{*}(z)\Gamma_j(\mathbf{q},z)\phi_{n'}(z) , \tag{16}$$

where $\Gamma_j(\mathbf{q},z)$ is[16] ($q=|\mathbf{q}|$)

$$I_j(\mathbf{q},z)=-\frac{i}{q}\left[\frac{e^2\varepsilon_0\hbar}{2\Omega_j(\mathbf{q})A}\right]^{1/2}E_{\parallel}^{j}(\mathbf{q},z)f_q . \tag{17}$$

In this formula $A=L^2$ is the area of the interface. $E_{\parallel}^{j}(\mathbf{q},z)$ is the lateral component of the electric field corresponding to the $j$th vibrational mode, with the wave vector $\mathbf{q}$. The screening function $f_q$ is identical to that used above in the case of the bulk approximation to the phonons.

For the purpose of further reference, let us write down the full Hamiltonian $H$ of the system under study, in the form of a sum of the unperturbed Hamiltonian $H_0$ and the perturbation $H_1$:

$$H=H_0+H_1,\quad H_0=H_e+H_{f\zeta},\quad H_1=H_{i\zeta} . \tag{18}$$

The index $\zeta=1$ and 2 refers, respectively, to the case of the bulk-phonon approximation, and the dielectric continuum model.

Other interactions, like, e.g., the anharmonic phonon-phonon interaction[11] or the coupling of electrons with other vibrational modes of the crystal lattice, will be neglected here. The electron-electron electrostatic interaction will be included implicitly by making the assumption that the electronic subsystem is thermalized.

## III. RATE EQUATIONS

In a process during which the hot phonons are produced in the course of the hot-electron cooling, the whole system is out of thermodynamic equilibrium. Such a process can be appropriately described by a theory of the nonequilibrium transport, as, for example, by the nonequilibrium Green-function theory,[33,34] or by the nonequilibrium statistical operator (NSO) theory.[35] The NSO theory will be used in this work.

For the case of not too fast changes of the nonequilibrium system, which is considered to be the case here, a reduced description of the nonequilibrium state is possible, according to which the nonequilibrium statistical operator $\rho(t)$ of the system can be expressed with help of a set $\{P_1,\ldots,P_r\}$ of operators $P_m$, used for the description of the system, the average values of which, at time $t$, are

$$\langle P_m\rangle=\mathrm{Tr}(\rho(t)P_m) . \tag{19}$$

An important role in the NSO theory is played by the auxiliary operator $\rho_q(t)$, called the quasiequilibrium operator, which is ascribed to any nonequilibrium state of the system. It is defined as

$$\rho_q(t)=\exp\left[\Phi(t)-\sum_{m=1}^{r}F_m(t)P_m\right] , \tag{20}$$

where $F_m(t)$ are determined by the equations

$$\langle P_m\rangle=\langle P_m\rangle_q^t , \tag{21}$$

where

$$\langle P_m\rangle_q^t=\mathrm{Tr}(\rho_q(t)P_m) . \tag{22}$$

$\Phi(t)$ is given by the normalization condition

$$\mathrm{Tr}(\rho_q(t))=1 . \tag{23}$$

The generalized kinetic equation in the NSO theory is the average of the corresponding Heisenberg equation, performed with the statistical operator $\rho(t)$. For weakly interacting systems a well-known expansion of $\rho(t)$ exists, in powers of the interaction $H_1$.[35] Neglecting certain memory terms and keeping the leading terms of the expansion of the collision integral, the kinetic equation giving the evolution of the mean value $\langle P_m\rangle$ is[35]

$$\frac{d}{dt}\langle P_m\rangle=S_m^{(0)}+S_m^{(1)}+S_m^{\prime(2)} , \tag{24}$$

where

$$S_m^{(0)}=\frac{1}{i\hbar}\langle[P_m,H_0]\rangle,\quad S_m^{(1)}=\frac{1}{i\hbar}\langle[P_m,H_1]\rangle_q^t \tag{25}$$

and

$$S_m^{\prime(2)}=-\frac{1}{\hbar^2}\int_{-\infty}^{0}dt_1e^{\varepsilon t_1}\langle[H_1(t_1),[H_1,P_m]]\rangle_q^t ,\qquad \varepsilon=0_+ , \tag{26}$$

in which

$$H_1(t)=\exp(iHt/\hbar)H_1\exp(-iHt/\hbar) . \tag{27}$$

The approximation of the full Hamiltonian $H$ in the latter equation, by the unperturbed Hamiltonian $H_0$ of free electrons and phonons, gives the Born approximation to the collision term $S_m^{\prime(2)}$ on the right-hand side of the kinetic equation (24). Later in this section, the first two terms on the right-hand side of Eq. (24) will be shown to be zero in the cases presently considered. Then performing the integration over $t_1$ in the term $S_m^{\prime(2)}$, one obtains ($\varepsilon=0_+$)

$$\frac{d}{dt}\langle P_m\rangle=\frac{i}{\hbar}\sum_{n,n',\mathbf{k},\sigma,\mathbf{q},q_z} A_{\mathbf{q},q_z} I_{n,n'}(q_z)\left[\frac{\langle[b_{\mathbf{q},q_z}c^{+}_{n,\mathbf{k},\sigma}c_{n',\mathbf{k}-\mathbf{q},\sigma},[H_1,P_m]]\rangle^{t}_{q}}{\epsilon_n(\mathbf{k})-\epsilon_{n'}(\mathbf{k}-\mathbf{q})-\hbar\omega_0-i\varepsilon}-\frac{\langle[b^{+}_{-\mathbf{q},-q_z}c^{+}_{n,\mathbf{k},\sigma}c_{n',\mathbf{k}-\mathbf{q},\sigma},[H_1,P_m]]\rangle^{t}_{q}}{\epsilon_n(\mathbf{k})-\epsilon_{n'}(\mathbf{k}-\mathbf{q})+\hbar\omega_0-i\varepsilon}\right]. \tag{28}$$

In the remaining part of this section the rate equations will be treated separately for the case of the bulk-phonon model and for the case of the dielectric continuum model.

### A. Bulk-phonon model

In the case of an inhomogeneous space distribution of hot LO phonons, the state of the phonon system can be described by the single-phonon density matrix $\langle b^{+}_{\mathbf{q},s_1}b_{\mathbf{q},s_2}\rangle$. In order to obtain the kinetic equation for this density matrix, it is suitable to include the operators $b^{+}_{q,s_1}b_{\mathbf{q},s_2}$ among the operators of the set $\{P_1,\ldots,P_r\}$. Assuming the LO phonons are dispersionless, the term $S_m^{(0)}$ is zero. The term $S_m^{(1)}$ is found to be a mean value of a product of particle operators, among which one, and only one, of the operators is a phonon operator. These terms will be set equal to zero. In the term $S_m'^{(2)}$, given by the right-hand side of Eq. (26), the commutators can be calculated and the resulting mean values decomposed with the help of the generalized Bloch–de Dominicis theorem.[36] In this procedure only terms like $\langle b^{+}_{\mathbf{q},q_z}b_{\mathbf{q},q_z'}\rangle$ and $\langle b_{\mathbf{q},q_z}b^{+}_{\mathbf{q},q_z'}\rangle$ are considered nonzero for arbitrary $q_z$ and $q_z'$. Introducing the notation

$$\nu_{\mathbf{q},q_z,q_z'}=\langle b^{+}_{\mathbf{q},q_z}b_{\mathbf{q},q_z'}\rangle \tag{29}$$

and

$$f_{n,\mathbf{k},\sigma}=\langle c^{+}_{n,\mathbf{k},\sigma}c_{n,\mathbf{k},\sigma}\rangle\ , \tag{30}$$

we arrive at the following equation for the evolution in time of the single-phonon density matrix:

$$\begin{aligned}\frac{d}{dt}\nu_{\mathbf{p},s_1,s_2}=&\frac{i}{\hbar}\sum_{n,n',\mathbf{k},\sigma,q_z} A_{\mathbf{p},q_z}A_{\mathbf{p},s_2}\frac{I_{n,n'}(q_z)I_{n',n}(-s_2)}{\epsilon_n(\mathbf{k})-\epsilon_{n'}(\mathbf{k}-\mathbf{p})-\hbar\omega_0-i\varepsilon}[f_{n,\mathbf{k},\sigma}(1-f_{n',\mathbf{k}-\mathbf{p},\sigma})\delta_{s_1,q_z}+(f_{n,\mathbf{k},\sigma}-f_{n',\mathbf{k}-\mathbf{p},\sigma})\nu_{\mathbf{p},s_1,q_z}]\\&-\frac{i}{\hbar}\sum_{n,n',\mathbf{k},\sigma,q_z} A_{p,s_1}A_{p,q_z}\frac{I_{n,n'}(s_1)I_{n',n}(-q_z)}{\epsilon_n(\mathbf{k})-\epsilon_{n'}(\mathbf{k}-\mathbf{p})-\hbar\omega_0+i\varepsilon}\\&\times[f_{n,\mathbf{k},\sigma}(1-f_{n',\mathbf{k}-\mathbf{p},\sigma})\delta_{q_z,s_2}+(f_{n,\mathbf{k},\sigma}-f_{n',\mathbf{k}-\mathbf{p},\sigma})\nu_{\mathbf{p},q_z,s_2}]\ .\end{aligned} \tag{31}$$

Assuming that the thermalization process within the electronic subsystem is fast enough, functions (30) are approximated by the Fermi-Dirac distribution function.

It is rather suitable to work with a more tractable concept than the matrix $\nu_{\mathbf{p},s_1,s_2}$. Recently, the generation of hot LO phonons was studied within the approximation of the bulk LO-phonon modes, basing on the concept of the phonon wave packet.[37,38] Equation (31) was obtained in Refs. 37 and 38 with the use of the method of Ref. 39. In the present paper the concept of the phonon wave packet will not be used; rather, the single-phonon density matrix will be expressed in terms of the Wigner distribution function.[33]

In the Q2D quantum well it is appropriate to introduce the function $N(\mathbf{p},q,z)$, defined as

$$N(\mathbf{p},q,z)=\frac{1}{V}\sum_{s}\nu_{\mathbf{p},q+(s/2),q-(s/2)}e^{-isz}\ . \tag{32}$$

This function has the properties of a Wigner function;[33] that is, it has the meaning of the number of the phonons in the vibrational mode $(\mathbf{p},q)$ having the momentum component $\mathbf{p}$ parallel to the $xy$ plane and the perpendicular momentum component $q$, in the unit volume of the coordinate space, placed at a distance $z$ from the $z=0$ plane. Because of the discretization of the vector $(\mathbf{p},q)$ which corresponds to the whole volume $V$ of the sample, only the quantity $VN(\mathbf{p},q,z)$ remains finite when $V\to\infty$. Obviously, at the thermal equilibrium of the phonon system at the lattice temperature $T_L$, it holds that

$$VN(\mathbf{p},q,z)=\nu_L=\frac{1}{\exp[\hbar\omega_0/(k_BT_L)]-1}\ . \tag{33}$$

For the purpose of the present paper it is suitable to introduce the nonequilibrium part $g(\mathbf{p},q,z)$ of $VN(\mathbf{p},q,z)$, i.e.,

$$g(\mathbf{p},q,z)=VN(\mathbf{p},q,z)-\nu_L\ , \tag{34}$$

and call it simply the Wigner function. When expressed in terms of the Wigner function, the rate equation (31) reads

$$\frac{d}{dt}g(\mathbf{p},q,z)=-\frac{2\pi}{\hbar}\sum_{n,n',\mathbf{k},\sigma,s}A_{\mathbf{p},q+(s/2)}A_{\mathbf{p},q-(s/2)}I_{n,n'}[q+(s/2)]I_{n',n}[-q+(s/2)]e^{-isz}$$
$$\times[f_{n,\mathbf{k},\sigma}(1-f_{n',\mathbf{k}-\mathbf{p},\sigma})+\nu_L(f_{n,\mathbf{k},\sigma}-f_{n',\mathbf{k}-\mathbf{p},\sigma})]\delta[\epsilon_n(k)-\epsilon_{n'}(\mathbf{k}-\mathbf{p})-\hbar\omega_0]+2\,\mathrm{Re}M(\mathbf{p},q,z)\ , \tag{35}$$

where

$$M(\mathbf{p},q,z)=\frac{iL}{\hbar}\sum_{n,n',q_z,s}\int_{-L/2}^{L/2}dz_1\,A_{\mathbf{p},q_z}A_{\mathbf{p},q-(s/2)}I_{n,n'}(q_z)I_{n',n}[-q+(s/2)]$$
$$\times e^{-isz}e^{i[q-q_z+(s/2)]z_1}g\left[\mathbf{p},\frac{q+q_z+\frac{s}{2}}{2},z_1\right]\Pi_{n,n'}(\mathbf{p})\ , \tag{36}$$

in which

$$\Pi_{n,n'}(\mathbf{p})=\frac{1}{L^2}\sum_{\mathbf{k},\sigma}\frac{f_{n,\mathbf{k},\sigma}-f_{n',\mathbf{k}-\mathbf{p},\sigma}}{\epsilon_n(\mathbf{k})-\epsilon_{n'}(\mathbf{k}-\mathbf{p})-\hbar\omega_0-i\varepsilon}\ . \tag{37}$$

Formula (35) is the second-order (in $H_1,\zeta=1$) expression for the generation rate of the LO phonons at a nonequilibrium state of the LO-phonon system, expressed by means of the Wigner function $g(\mathbf{p},q,z)$. The term $M(\mathbf{p},q,z)$ contributes to the generation rate of the hot-phonon population when the state of the phonon system differs from the equilibrium state $\nu_L$. The hot-phonon effect is neglected in the present work upon taking the term $M(\mathbf{p},q,z)$ as zero.

In a completely analogical way the rate of the change of the total electronic energy $\langle H_e\rangle$ can be obtained from Eq. (28). The result is

$$\frac{d}{dt}\langle H_e\rangle=-2\pi\omega_0\sum_{n,n',\mathbf{k},\mathbf{q},q_z,\sigma}|A_{\mathbf{q},q_z}|^2|I_{n,n'}(q_z)|^2[f_{n,\mathbf{k},\sigma}(1-f_{n',\mathbf{k}-\mathbf{q},\sigma})+\nu_L(f_{n,\mathbf{k},\sigma}-f_{n',\mathbf{k}-\mathbf{q},\sigma})]\delta[\epsilon_n(\mathbf{k})-\epsilon_{n'}(\mathbf{k}-\mathbf{q})-\hbar\omega_0]$$
$$+\frac{2\pi\omega_0}{L}\sum_{\mathbf{k},\mathbf{q},q_z,q_z'}\int_{-L/2}^{L/2}dz\,A_{\mathbf{q},q_z}A_{\mathbf{q},q_z'}I_{n,n'}(q_z')I_{n',n}(-q_z)e^{i(q_z-q_z')z}$$
$$\times g\left[\mathbf{q},\frac{q_z+q_z'}{2},z\right](f_{n,\mathbf{k},\sigma}-f_{n',\mathbf{k}-\mathbf{q},\sigma})\delta[\epsilon_n(\mathbf{k})-\epsilon_{n'}(\mathbf{k}-\mathbf{q})-\hbar\omega_0]\ . \tag{38}$$

This is the second-order (in $H_1,\zeta=1$) formula for the rate of change of the mean electronic energy, expressed in terms of the Wigner function, valid for a nonequilibrium state of the phonon system. It is straightforward to see that

$$\frac{d}{dt}\langle H_e\rangle=-\frac{\hbar\omega_0}{L}\sum_{\mathbf{p},q_z}\int_{-L/2}^{L/2}dz\frac{d}{dt}g(\mathbf{p},q_z,z)\ . \tag{39}$$

Let us define the zeroth moment $g_0(\mathbf{p},q_z)$ of the Wigner distribution function $g(\mathbf{p},q_z,z)$ as

$$g_0(\mathbf{p},q_z)=\frac{1}{d}\int_{-L/2}^{L/2}g(\mathbf{p},q_z,z)dz\ , \tag{40}$$

which is related to the diagonal part of the single-phonon density matrix (29).[40] At least in sufficiently broad quantum wells the nonzero values of the Wigner function are confined roughly to the interval $-d/2<z<d/2$, which appears to be supported by additional numerical computations. The function $g_0(\mathbf{p},q_z)$ then has the meaning of an average of the Wigner function $g(\mathbf{p},q_z,z)$ in the area of the quantum well. The rate of change of the mean electronic energy is then given in fact by the rate of change of the zeroth moment of the Wigner function,

$$\frac{d}{dt}\langle H_e\rangle=-\frac{\hbar\omega_0 d}{L}\sum_{\mathbf{p},q_z}\frac{d}{dt}g_0(\mathbf{p},q_z)\ . \tag{41}$$

The hot-phonon population of a semiconductor quantum well can be conveniently monitored with help of the Raman-scattering experiment. The signal which is measured in this experiment is, in general, given by the full single-phonon density matrix or by the corresponding Wigner distribution function. It is, however, reasonable to expect that the leading contribution to the Raman signal, due to the nonequilibrium phonon population, will be given by the zeroth moment $g_0(\mathbf{p},q)$ of the Wigner function $g(\mathbf{p},q,z)$ at the quantum-well widths considered here.

Under the condition that the electrons are at equilibrium at the temperature $T_e$, while the phonons are at equilibrium at the temperature $T_L$, it is obtained from Eq. (35) that the generation rate of the zeroth moment of the Wigner func-

tion reads

$$\frac{d}{dt}g_0(\mathbf{p},q_z)=\frac{2\pi L}{\hbar d}\sum_{n,n'}|A_{\mathbf{p},q_z}|^2|I_{n,n'}(q_z)|^2\sum_{\mathbf{k},\sigma}[f_{n,\mathbf{k},\sigma}(1-f_{n',\mathbf{k}-\mathbf{p},\sigma})+\nu_L(f_{n,\mathbf{k},\sigma}-f_{n',\mathbf{k}-\mathbf{p},\sigma})]\delta[\epsilon_n(\mathbf{k})-\epsilon_{n'}(\mathbf{k}-\mathbf{p})-\hbar\omega_0]\ . \tag{42}$$

The rates of change of the zeroth moment of the phonon Wigner function and of the mean electronic energy, given by Eqs. (42) and (41), respectively, will be evaluated numerically later in this paper.

### B. Dielectric continuum model

Similarly to the case of the bulk approximation to the optical phonons, we confine ourselves to the Born approximation to the collision integral $S_m'^{(2)}$. At a nonequilibrium, the state of the phonon system can be described by the single-phonon density matrix $\Phi_{jl}(\mathbf{q})$,

$$\Phi_{jl}(\mathbf{q})=\langle a_j^+(\mathbf{q})a_l(\mathbf{q})\rangle\ . \tag{43}$$

Generally, the hot-phonon signal, detected in the Raman-scattering experiment, will be determined by the matrix $\Phi_{jl}(\mathbf{q})$. It is assumed here that, to a good approximation, the detected signal is determined by the diagonal terms $\Phi_l(\mathbf{q})=\Phi_{ll}(\mathbf{q})$ of the full density matrix $\Phi_{jl}(\mathbf{q})$. In the kinetic equation for the diagonal term $\Phi_l(\mathbf{q})$ the term $S_m^{(0)}$ is obviously zero. The term $S_m^{(1)}$ is set equal to zero, using argumentation analogical to that used in Sec. III A. With Hamiltonian (18), where $\zeta=2$, it is obtained that

$$\frac{d\Phi_l(\mathbf{q})}{dt}=\frac{i}{\hbar}\sum_{n,n',\sigma,\mathbf{p},j}\gamma_j^{n,n'}(\mathbf{q})\gamma_l^{n',n}(-\mathbf{q})\frac{\delta_{jl}f_{n,\mathbf{p}+\mathbf{q},\sigma}(1-f_{n',\mathbf{p},\sigma})+\Phi_{lj}(\mathbf{q})(f_{n,\mathbf{p}+\mathbf{q},\sigma}-f_{n',\mathbf{p},\sigma})}{\hbar\Omega_j(\mathbf{q})-\epsilon_n(\mathbf{p}+\mathbf{q})+\epsilon_{n'}(\mathbf{p})+i\varepsilon}$$
$$-\frac{i}{\hbar}\sum_{n,n',\sigma,\mathbf{p},j}\gamma_l^{n,n'}(\mathbf{q})\gamma_j^{n',n}(-\mathbf{q})\frac{\delta_{jl}f_{n,\mathbf{p}+\mathbf{q},\sigma}(1-f_{n',\mathbf{p},\sigma})+\Phi_{jl}(\mathbf{q})(f_{n,\mathbf{p}+\mathbf{q},\sigma}-f_{n',\mathbf{p},\sigma})}{\hbar\Omega_j(-\mathbf{q})-\epsilon_n(\mathbf{p}+\mathbf{q})+\epsilon_{n'}(\mathbf{p})-i\varepsilon}\ . \tag{44}$$

When the phonon system is at equilibrium, then $\Phi_{jl}(\mathbf{q})$ on the right-hand side of the latter equation, in which it may represent the hot-phonon effect, is diagonal and the generation rate reduces to terms proportional to the energy-conserving $\delta$ function, which have the meaning of the phonon generation due to the hot-electron cooling. When $\Phi_{jl}(\mathbf{q})$ is not diagonal, then Eq. (42) also contains terms, the meanings of which are a redistribution of the hot phonons in space.

Restricting ourselves to considering the phonon generation rate in the state at which the electrons have the temperature $T_e$ and the phonons have the temperature $T_L$, the generation rate $d\Phi_j(\mathbf{q})/dt$ is then

$$\frac{d\Phi_j(\mathbf{q})}{dt}=\frac{2\pi}{\hbar}\sum_{\mathbf{p},\sigma,n,n'}|\gamma_j^{n,n'}(\mathbf{q})|^2\delta[\hbar\Omega_j(\mathbf{q})-\varepsilon_n(\mathbf{p}+\mathbf{q})+\varepsilon_{n'}(\mathbf{p})]$$
$$\times\{f_{n,\mathbf{p}+\mathbf{q},\sigma}(1-f_{n',\mathbf{p},\sigma})[1+\Phi_j(\mathbf{q})]-f_{n',\mathbf{p},\sigma}(1-f_{n,\mathbf{p}+\mathbf{q},\sigma})\Phi_j(\mathbf{q})\}\ , \tag{45}$$

while the rate of change of the electronic energy at this state of the whole system is

$$\frac{d\langle H_e\rangle}{dt}=-\sum_{j,\mathbf{q}}\hbar\Omega_j(\mathbf{q})\frac{d\Phi_j(\mathbf{q})}{dt}\ . \tag{46}$$

The latter two formulas will be evaluated numerically.

## IV. NUMERICAL RESULTS AND DISCUSSION

The electrophonon resonance effect will be analyzed numerically assuming that the electron-phonon system is prepared at a state at which the electrons have a temperature $T_e$ and a (three-dimensional) density $n_e$, while the lattice vibrational modes have a temperature $T_L, T_L<T_e$, by the action of a short laser pulse at some instant of time. In Sec. IV A the electrophonon resonance based on the phonon generation rate is evaluated. The hot-electron cooling rate electrophonon resonance is considered in Sec. IV B. The numerical computations are performed using the material parameters taken over from Refs. 41, 42, and 43. In particular, in GaAs we take[42,43]

$$\kappa_{\infty 1}=10.90,\quad \omega_{L1}=5.496\times10^{13}\ \mathrm{s}^{-1}\ ,$$
$$\omega_{T1}=5.057\times10^{13}\ \mathrm{s}^{-1}\ ,$$

while for $Al_{0.25}Ga_{0.75}As$ we use

$$\kappa_{\infty 2}=10.22,\quad \omega_{L2}=6.979\times10^{13}\ \mathrm{s}^{-1}\ ,$$
$$\omega_{T2}=6.731\times10^{13}\ \mathrm{s}^{-1}\ .$$

### A. LW-phonon generation

#### 1. *Bulk-phonon model*

Because of the isotropy of the generation rate with respect to the direction of the lateral component of the wave vector $\mathbf{p}$, this rate is computed for $\mathbf{p}=(p,0)$ and is denoted as $dg_0(p,q)/dt$. Five electronic subbands are

taken into account. The lattice temperature is $T_L=10$ K. The hot-phonon generation rate $dg_0(p,q)/dt$ is given in Fig. 1 as a function of the lateral component of the wave vector $p$ and the normal component $q$ of the LO phonon. This generation rate is computed at such a well width (150 Å), at which no pair of the subband energies $E_n$ is at resonance with the energy of the LO phonons. This can be verified upon inspection of Table I. In this table those well widths are given at which the resonance conditions

$$E_n - E_{n'} = \hbar\omega_0 \tag{47}$$

is fulfilled by a pair of electronic subband energies $E_n$ and $E_{n'}$. The squares of the absolute values of the form factors, $|I_{n,n'}(q)|^2$, are also given in Table I, computed for $q=q_c=0.7\times10^8$ m$^{-1}$. The reason for this choice of wave vector $q$ will become clear below. Thus, as can be seen in Fig. 1, below about $p=0.25\times10^8$ m$^{-1}$, the hot phonons are not generated, consistently with the fact that the resonance condition is not fulfilled.

In Fig. 2 the phonon generation rate is computed at the well width of $d=216$ Å, at which the resonance between the second and first electronic subbands occurs (see Table I). At this situation the phonons with a small lateral component of the wave vector are strongly generated. This is manifested by the presence of a narrow ridge in Fig. 2 at about $p=0.05\times10^8$ m$^{-1}$. Detailed computations show that when the resonance condition is fulfilled, the ridge is very narrow, and is found very close to the $p=0$ plane. The ridge moves away from the $p=0$ plane, and becomes broader, subsequently, as the well width increases.

In the current applications of the Raman-scattering technique, for the study of the hot-phonon population in quantum wells, the geometry of the possible experimental setup, as determined by the Brewster angle restrictions, is reported[7-9] to be such that the momentum of the detected nonequilibrium phonons is about $p_c=0.05\times10^8$ m$^{-1}$ in the lateral direction, while in the direction normal to the quantum-well interfaces the phonon momentum component is about $q_c=0.7\times10^8$ m$^{-1}$ (backward scattering). Assuming, as was done already above, that the intensity of the Raman signal is basically determined by the zeroth moment of the Wigner function, we shall analyze further the generation rate $dg_0(p_c,q_c)/dt$. From this reason the form factor in Table I is computed at the value of $q=q_c$. The generation rate $dg_0(p_c,q_c)/dt$ will be computed as dependent on the well width and on a homogeneous electric field applied in the direction normal to the interfaces of the well. The occurrence of the Raman signal is then expected to mark the onset of the intersubband optical-phonon scattering between a pair of subbands.

TABLE I. Resonance well widths (in $10^{-10}$ m) and form factors.

| $d$ | $n$ | $n'$ | $\lvert I_{n,n'}(q_c)\rvert^2$ |
|---|---|---|---|
| 216 | 2 | 1 | 0.07 |
| 279 | 3 | 2 | 0.12 |
| 330 | 4 | 3 | 0.17 |
| 353 | 3 | 1 | 0.01 |
| 374 | 5 | 4 | 0.20 |
| 414 | 6 | 5 | 0.23 |
| 432 | 4 | 2 | 0.03 |
| 450 | 7 | 6 | 0.25 |
| 483 | 8 | 7 | 0.27 |
| 483 | 4 | 1 | $5\times10^{-5}$ |
| 499 | 5 | 3 | 0.06 |

In Figs. 3–5 the generation rate $dg_0(p_c,q_c)/dt$ is computed at the values of $p_c$ and $q_c$ given above. In Fig. 3 the generation rate is presented as a function of the width $d$ of the quantum well. Comparing the resonance well widths, at which the generation rate achieves the maxima, with the well widths given in Table I, it can be seen that the positions of the resonance maxima of the generation rate correspond practically exactly with the well widths given in Table I. It appears that the observation of the resonance at $p=p_c$, instead at $p=0$, causes an error in the determination of the resonance well width, which is not larger than about $10^{-10}$ m, in the range of the well widths of Fig. 3.

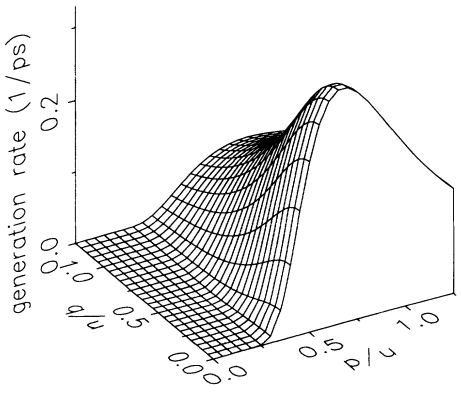


FIG. 1. Generation rate $d_0(p,q)/dt$ as a function of the lateral component $p$ and normal component $q$ of phonon wave vector ($u=10^8$ m$^{-1}$), $T_e=1000$ K, $T_L=10$ K, and $n_e=10^{22}$ m$^{-3}$. The well width is 150 Å.

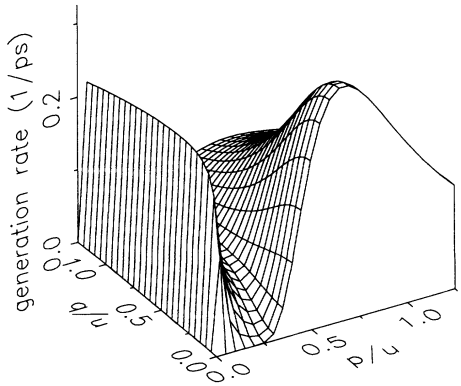


FIG. 2. Generation rate $dg_0(p,q)dt$ at the well width of 216 Å. See the caption to Fig. 1 for other data.

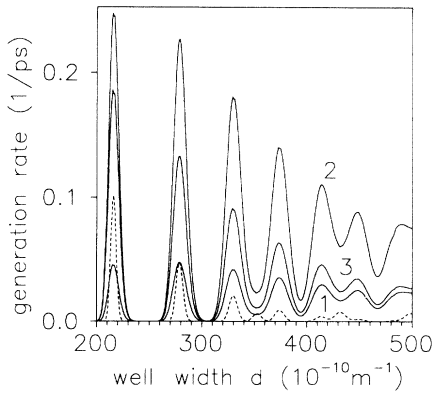


FIG. 3. Generation rate $dg_0(p_c,q_c)/dt$ as a function of the well width, at $p_c=0.05\times10^8$ m$^{-1}$ and $q_c=0.7\times10^8$ m$^{-1}$. Solid lines: $T_e=1000$ K and $T_L=10$ K. The electronic densities $n_e$ are $10^{21}$ m$^{-3}$ (curve 1), $10^{22}$ m$^{-3}$ (curve 2), and $10^{23}$ m$^{-3}$ (curve 3). These lines conserve their mutual ordering throughout the graph. Dashed line: $T_e=300$ K, $T_L=10$ K, and $n_e=10^{22}$ m$^{-3}$.

In Fig. 3 the $d$ dependence of the generation rate $dg_0(p_c,q_c)/dt$ is displayed for three values of the electronic density $n_e$. From the point of view of the magnitude of the generation rate, or the nonequilibrium phonon population, there appears to be an optimal value of the electronic density. The decrease of the computed population at the density roughly above $10^{22}$ m$^{-3}$ can be explained by the increase of the influence of the static screening with the increase of the electronic density.

The width of the resonant peaks, displayed in Fig. 3, appears to depend on the temperature $T_e$ of the electronic system. With decreasing $T_e$ the width of the resonance peak decreases, together with the generation rate. It is observed that there is a correlation between the values of $|I_{n,n'}(q)|^2$, corresponding to a given resonance, as given in Table I, with the strength of the corresponding peak in Fig. 3.

The high sensitivity of the LO-phonon generation rate $dg_0(p_c,q_c)/dt$ to the variation of the well width allows

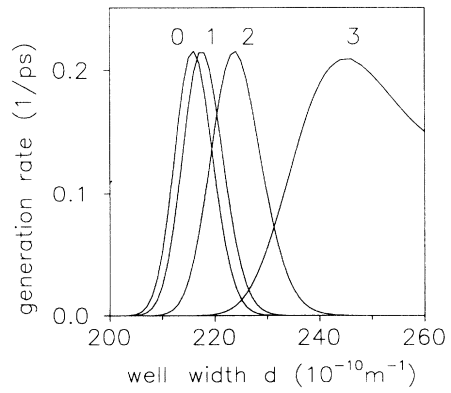


FIG. 4. Generation rate $dg_0(p_c,q_c)/dt$ as a function of the well width, $T_e=600$ K, $T_L=10$ K, and $n_e=10^{22}$ m$^{-3}$. Electric-field intensity $F$ in units of $10^7$ V/m: 0 (curve 0), 0.1 (curve 1), 0.2 (curve 2), and 0.3 (curve 3).

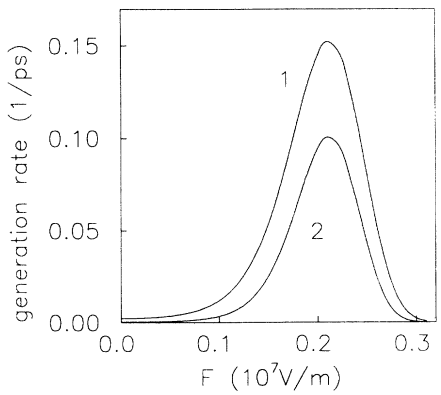


FIG. 5. Generation rate $dg_0(p_c,q_c)/dt$ as a function of the electric-field intensity $F$, at the well width $d=225$ Å and $T_L=10$ K. Curve 1, $T_e=400$ K; curve 2, $T_e=300$ K.

one to expect that the sensitivity of the same quantity to a homogeneous and constant electric field, applied in the normal direction, will be similarly high. For the sake of simplicity, the influence of the electric field on the electronic energies and electronic wave functions in the quantum well is taken into account only by means of the standard perturbation theory calculation.[44] Because of the restrictions imposed by the limits of validity of the perturbation theory, the influence of the electric field is displayed only for a restricted range of well widths. The numerical results are illustrated in Fig. 4. The resonance maximum, which is located at $d=216$ Å at the zero electric field, shifts toward higher values of $d$ with increasing electric-field strength. The magnitude of the shift in $d$ appears to be roughly quadratic in the electric-field strength $F$, as expected in the quantum well considered, with the potential profile being symmetrical with respect to the reflection in the $z=0$ plane.

The modulation of the generation rate with the variation of the electric-field intensity is shown in Fig. 5. In this figure the phonon generation rate $dg_0(p_c,q_c)/dt$ is plotted against the electric-field intensity $F$, at a well width of 225 Å. A comparison of the two curves in Fig. 5, computed at different temperatures of the electronic subsystem, shows again that the width of the resonance pattern decreases with decreasing $T_e$, together with the overall decrease of the generation rate. The data presented in both Figs. 5 and 3 show that the modulation of the long wavelength population in the electrophonon resonance effect, controlled by varying either the well width or the electric field, may be rather strong.

### 2. *Dielectric continuum model*

Similarly to the case of the bulk-phonon model, the phonon distribution function is considered dependent only on the magnitude $q$ of the wave vector $\mathbf{q}$. In Fig. 6 the generation rate $d\Phi_l(q)/dt$, computed at the fixed value of $q=0.05\times10^8$ m$^{-1}$, the choice of which is based on similar argumentation to that given in the Sec. IV A 1, displays a strong modulation with respect to the variation of the well width for both the interface and the confined modes. Seven electronic subbands are taken into account

in the numerical calculation. In this section the computations are carried out at $n_e=10^{22}$ m$^{-3}$ and $T_L=4.2$ K. In Fig. 6(a) the generation rate is displayed for the confined modes. In the presently used theory of optical phonons, the frequencies of the confined modes are identical to the frequencies of the LO modes of bulk GaAs, $\Omega_m(q)=\omega_0$, for $m=1,2,\ldots$. The well widths at which it holds that

$$\hbar\Omega_m(q)=E_n-E_{n'}, \tag{48}$$

for a pair of electron subbands $n$ and $n'$, are identical with those given in Table I. Similarly to the case of the bulk-phonon model, it holds here that the positions of the resonance maxima in Fig. 6(a) agree with high accuracy (less than 1 Å) with the resonant well widths given in Table I. Restricting ourselves to the first five well widths given in Table I, in agreement with the symmetry restrictions, the $m=2$ and 4 confined modes give the resonances at these well widths, with the exception of the resonance at $d=353$ Å. At this particular well width only, the symmetrical phonon modes with $m=1$, 3, and 5 provide the resonant spikes.

Note the similarity between this figure and Fig. 3 containing the electrophonon resonance pattern calculated in the bulk-phonon model. The dielectric continuum model allows for a more detailed classification of the peaks in the resonance pattern. The intensities of the resonant maxima calculated within the two phonon models are rather close to each other for the confined modes with even $m$, while the resonance feature at $d=353$ Å, corresponding to the odd values of $m$, comes out rather weak in the bulk-phonon model calculation.

The resonance pattern due to the interface modes of $d\Phi_l(q)/dt$ plotted against the well width, is displayed in Fig. 6(b). It appears that the strongest phonon generation rate can be expected for the mode ($A-$). The positions of the resonant peaks practically agree with those of the antisymmetrical confined modes ($m=2$ and 4), which is due to the fact that the energy of the ($A-$) phonon is close to the energy of the confined phonon. The intensity of the resonant maxima due to the ($A-$) mode comes out as comparable to the intensity of the confined modes. Generally speaking, when using a resonant condition of the type of Eq. (48) in the case of the interface modes, one should be aware of the wave-vector dependence of the interface phonon energy. Nevertheless, one can argue that because the energy of the ($A+$) mode appears to be larger[31] than $\hbar\omega_0$, the resonance maxima of this antisymmetrical interface mode come out systematically at lower values of the well width. The generation rate due to this $Al_xGa_{1-x}As$ mode is smaller than the rate due to the ($A-$) mode, however. The resonance peaks due to the symmetrical interface modes, expected at about 353 Å, between the electronic subbands $n=3$ and $n'=1$, are very weak and could thus not be shown in this figure.

The generation rates of the distribution functions, plotted against the wave vector $q$, are displayed for several significant phonon modes and well widths in Fig. 7. Curves 1–4 show the generation rates of the respective modes at such well widths, at which the resonance condition (48) for the intersubband scattering is fulfilled. All these curves have their maxima at low values of $q$, and decrease quickly with increasing $q$. Figure 7, together with Figs. 1 and 2, show that at long wavelengths the

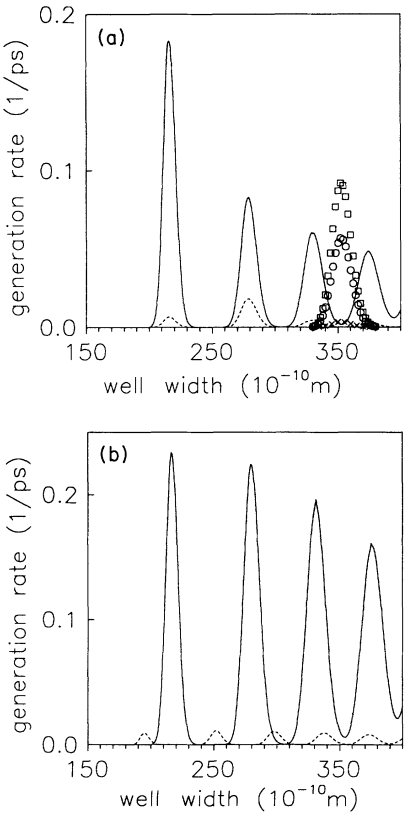


FIG. 6. Generation rate $d\Phi_l(q)/dt$ as a function of the well width, at $q=0.05\times10^8$ m$^{-1}$, $T_e=1000$ K, $T_L=4.2$ K, and $n_e=10^{22}$ m$^{-3}$. (a) Confined modes. Circles: $m=1$; full line: $m=2$; squares: $m=3$; dashed line: $m=4$; crosses: $m=5$. (b) Interface modes. Full line: mode ($A-$); dashed line: mode ($A+$).

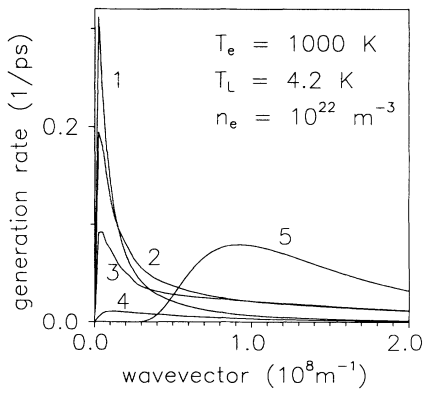


FIG. 7. Generation rate $d\Phi_l(q)/dt$ as a function of the wave vector $q$, at $T_e=1000$ K, for the following modes and well widths: curve 1: interface ($A-$), $d=217$ Å; curve 2: confined $m=2$, $d=217$ Å; curve 3: confined $m=3$, $d=353$ Å; curve 4: interface ($A+$), $d=194$ Å, curve 5; confined $m=1$, $d=217$ Å.

generation rates of the interface modes, and therefore also the hot-phonon populations of the interface modes, can be expected to be comparable to those of the confined (or bulk) modes, even at well widths of about 200 Å or larger. The decrease of the generation rate of the ($A+$) mode, with increasing $q$, is relatively slow. This is due to the fact that the wave-vector dependence of the frequency of this mode is an increasing function of a $q$.[31] This property influences the resonance condition in such a way that the range of the wave vector $q$, for which the resonance condition is fulfilled, tends to broaden. It is observed that the overall trend of the LO-phonon generation rate, observed in the above-considered bulk-phonon model, namely to give a strong generation in the long-wavelength area under resonant conditions, is repeated here, even in the case of the interface modes.

For the purpose of comparison, the generation rate of the confined mode with $m=1$ (curve 5) at $d=217$ Å is shown. At this well width, this mode takes part only in the intraband optical-phonon scattering processes of a nonresonant nature. The energy and momentum conservation laws, which restrict the intraband scattering, together with the form of the electronic distribution function, lead to the appearance of the usual maximum of the generation rate at about $q=10^8$ m$^{-1}$ and to the absence of the phonon generation in the region $q<0.3\times10^8$ m$^{-1}$ of the phonon wave vector.

A static and homogeneous electric field, applied to the quantum-well system with the intensity $F$ normal to the interfaces, causes changes in the energy levels and wave functions of the electronic motion in the normal direction. Because of the limited validity of the standard perturbation theory,[44] used in the present case, the electrophonon resonance effect is considered only in such cases in which the phonon energy comes into resonance with the lowest two electronic subband energies $E_1$ and $E_2$. As was shown above in the case of the bulk-phonon model, under the influence of the electric field the resonant peaks move toward larger values of the well widths in plots of the generation rate such as those in Figs. 6(a) and 6(b). In order that a low enough electric field be sufficient for the demonstration of the electrophonon resonance effect, a suitable choice of well width is again necessary. In Fig. 8(a), the latter effect is demonstrated for the case of the confined phonon mode with $m=2$, choosing a well width equal to 235 Å. The plot of $d\Phi_l(q)/dt$ at $q=0.05\times10^8$ m$^{-1}$ against the electric-field intensity $F$ shows that a distinct resonance pattern with a well-defined maximum and with the generation rate decreasing sharply toward zero at both the high- and low-field sides of the resonance peak can already be observed in the field range up to $0.5\times10^7$ V/m. This result is supported by the bulk model calculation of Sec. IV A 1, which leads to a similar conclusion. Similarly, a decrease of the electronic temperature leads to a narrowing of the electrophonon resonance maximum; however, the overall intensity of the generation rate decreases as well.

In the same Fig. 8(a) a plot is displayed of the electrophonon resonance between the electronic levels $E_1$ and $E_2$ and the energy of the interface mode ($A-$) at a well width of 235 Å. Because of the close values of the energies of the confined phonon and the interface phonon ($A-$), these two modes cannot be practically distinguished according to the position of the resonant maximum on the field axis. However, the intensity of the rate due to the interface mode ($A-$) is expected to be as strong as that due to the confined modes, at this well width. In Fig. 8(b) the same plot of the generation rate of the ($A+$) mode, taken at a well width of 205 Å, shows similar characteristics, as far as the field dependence of the generation rate is concerned. A nonperturbative treatment of the electric field would be suitable in order that the electrophonon resonance be demonstrated theoretically in more detail at larger well widths and/or stronger electric fields.

### B. Hot-electron cooling rate

The electrophonon resonance based on the hot-electron cooling rate is evaluated numerically under similar conditions as assumed in previous sections; that is at the initial instant of time of the process of the hot-electron relaxation, at which the electron subsystem is prepared at the state with temperature $T_e$, while the phonons are at equilibrium at the temperature of the ambient lattice $T_L$. The three-dimensional electronic density $n_e$ is kept con-

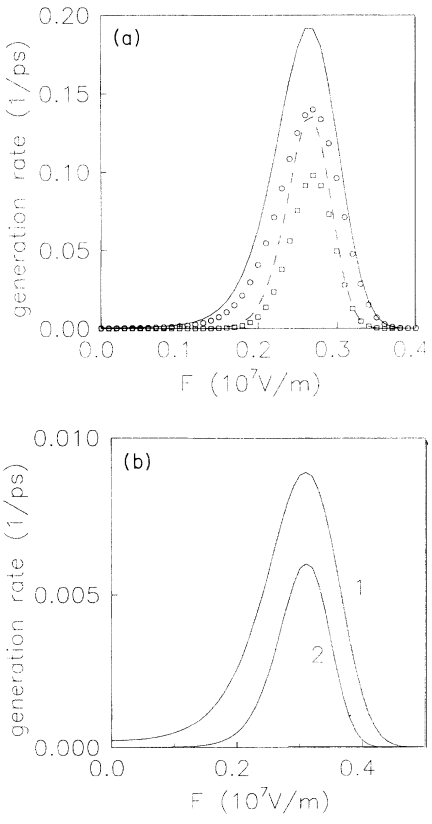


FIG. 8. Generation rate $d\Phi_l(q)/dt$ as a function of electric field $F$, at $q=0.05\times10^8$ m$^{-1}$. (a) Well width of 235 Å. Confined mode with $m=2$ at $T_e=1000$ (circles) and 500 K (squares); interface mode ($A-$) at $T_e=1000$ (full line) and 500 K (dashed). (b) Well width of 205 Å, interface mode ($A+$). Curve 1: $T_e=1000$ K; curve 2: $T_e=500$ K.

stant throughout the calculation and equal to $10^{22}$ $m^{-3}$. The temperature $T_L$ of the phonon system is set equal to 4.2 K. Both the dielectric continuum model and the bulk-phonon model are used in this section. The number of the electronic subbands taken into account is five in the present section. The first five modes of the confined phonons are included. The power loss $r$ per one electron can be expressed as $r=-(Vn_e)^{-1}(d\langle H_e\rangle/dt)$.

In Figs. 9 and 10 the $d$ dependence of the power loss is presented, calculated within the dielectric continuum model. The cooling rate computed at $T_e=50$ K is given in Fig. 9. The power loss per electron $r$, expressed in pW per electron, appears to reach a broad maximum at about 70–80 Å (1 Å$=10^{-10}$ m). The presence of this maximum, which is a nonresonance one, however, is linked to the interplay between the increasing efficiency of the coupling between electrons and confined phonons on one side, and the decrease of the electron population of the lowest subband on the other side, when $d$ is increased. The maximum at about 220–240 Å corresponds to electrophonon resonance of the two lowest electronic subbands with the optical phonons. This maximum does not reveal any structure due to the difference between confined and interface phonons. Another resonance is seen at a range of well widths of 350–360 Å. At this resonance, the first and third electronic subbands are at resonance with the single-phonon energies. Additional computation shows that this resonance feature, together with a number of others, appear to be systematically weaker than the feature at 220–240 Å and will thus not be discussed in detail. In particular, the interface modes play a negligible role at these resonances.

The resonance curve of $r$ as a function of the well width $d$, computed with the electronic screening included, shows that the screening provides not only an overall decrease of the hot-electron rate, but also that it makes the resonance maxima less pronounced. The latter effect is caused by the fact that the processes of the generation of the long-wavelength optical phonons, which become

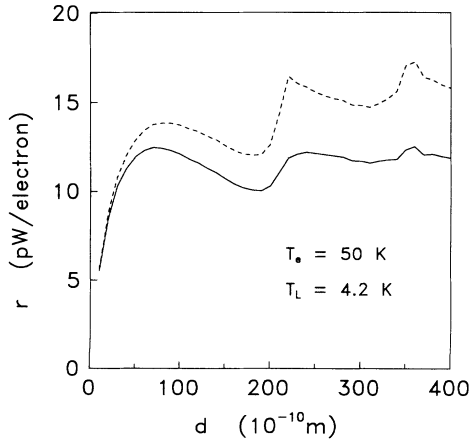


FIG. 9. Power loss per electron $r$ as a function of well width $d$ in $Al_xGa_{1-x}As$-GaAs quantum well. Five lowest electronic subbands, five confined modes and all interface modes are included (full line). Dashed line, without screening.

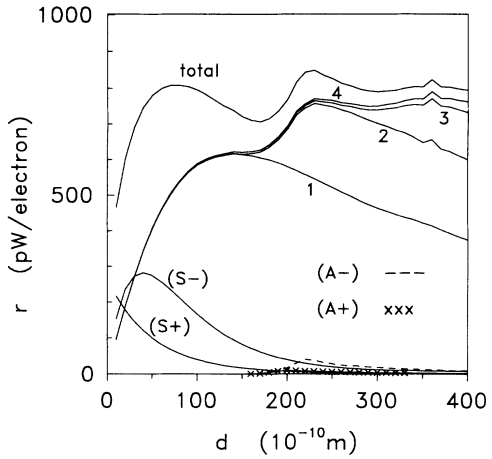


FIG. 10. Separate contributions of the interface modes $(S-)$, $(S+)$, $(A-)$, and $(A+)$ to the power loss per electron. Number $n$ at the curves means the separate contribution due to first $n$ confined modes only. $T_e=100$ K. All vibrational modes are included (five confined modes) in the total curve.

effective upon the onset of the RISOPS between the two subbands, and which lead to the well-developed spikes at the resonances, are suppressed by the screening. The unscreened power loss in Fig. 9 should be compared with the cooling rate given recently in Ref. 6, computed within the bulk-phonon model. On comparison one can see that the appearance of well-developed spikes in the cooling rate is connected with the absence of the electronic screening of Fröhlich interaction at long phonon wavelengths. Let us remark that the resonance pattern of the $d$ dependence of electron mobility in the $Al_xGa_{1-x}As$-GaAs quantum well, given in Refs. 4 and 5, which is reported to be calculated without electronic screening, does not reveal a sharp-peak structure. Similarly, the $d$ dependence of the electron mobility in a GaAs slab, calculated[45] with the use of bulk phonons, without electronic screening, does not possess a sharp-spike structure at comparable electronic densities and lattice temperature. This may lead to a conclusion that the electron mobility resonance pattern can be expected to be less pronounced than the hot-electron cooling rate resonance pattern.

The structure of the cooling rate resonance pattern is further analyzed in Fig. 10, in which the individual optical-phonon mode contributions are identified. The interface phonons clearly have a dominating role at $d=20$ Å. Their contribution to the hot-electron cooling rate prevails over that of the confined phonons until about $d=50$ Å. This appears to be in accord with recent experimental findings[10] for GaAs-AlAs quantum wells. The contribution of the interface phonons decreases with increasing $d$, while the contribution of the confined modes increases. The position of the cooling rate maximum at 70–80 Å is influenced by both interface modes and one $(m=1)$ confined mode. At 200 Å the contribution of the interface modes is about 10% of the total cooling rate due to all phonon modes taken into account.

The resonant feature at about 230 Å, at which the two lowest electronic subbands are at resonance with the

optical-phonon energies, is due mostly to $m=2$ confined mode. The two antisymmetrical interface modes which contribute to this resonance are ($A+$) and ($A-$). The energy of ($A-$) mode appears to be quite close to the energy of LO phonons of bulk GaAs. This is why the resonance contribution due to this mode is positioned quite close to that of the confined mode. Although this mode is the one which is more strongly coupled, out of the two antisymmetrical confined modes the resonance maximum due to this mode remains hidden on the background of the $m=2$ confined mode. The contribution of the $Al_xGa_{1-x}As$ interface mode ($A+$) at 190 Å is separated enough on a scale of $d$ to be distinguished from the main feature at 230 Å; however, it comes out to be very weak.

Besides Fig. 9, in which the effect of the electronic screening is computed with the use of the dielectric continuum model, this effect is also displayed in Fig. 11, computed with the use of the bulk-phonon model. In Fig. 11 the power loss per electron is plotted as a function of the well width. Similarly to the case of the dielectric continuum model (Fig. 9), the introduction of the static screening leads not only to an overall decrease of the hot-electron cooling rate, but also to a loss of the sharpness of the resonance spikes with respect to the resonance pattern computed without the electronic screening. Curves 1, 2, and 3 in Fig. 11 shows the effect of the electric field on the hot-electron cooling rate resonance pattern. The peak, which is positioned at 216 Å in the absence of the field, shifts toward higher values of $d$, and the high-$d$ shoulder of it increases with the increase of the field intensity. This behavior can be understood upon realizing that, besides the electronic energies, the electronic wave functions also are influenced by the electric field, which in turn has an impact on the electron-phonon scattering via the form factors (10). Also, the applied electric field influences the nonresonant background in the resonant pattern displayed in Fig. 11. A more detailed quantitative analysis of the influence of the electric field on the hot-electron cooling rate would require a nonperturbative treatment of the electric field, although it is quite obvious that the electrophonon resonance effect based on the hot-electron cooling rate, controlled by the normal electric field, is likely to be less pronounced than that based on the direct long-wavelength optical-phonon detection.

As we have seen, the interface phonons are not likely to be easily distinguished in both hot-electron cooling rate and electronic mobility resonance patterns in the rectangular $Al_xGa_{1-x}As$-GaAs quantum wells presently considered. The main reason for this is the large well width $d$ at which the resonance separation of the electronic subbands is achieved, at which the contributions of the interface modes are already relatively weak. An otherwise sufficiently simple quantum-well structure, at which at least one of the subband electronic wave functions $\phi_n(z)$ overlaps sufficiently with the interface modes, would be more favorable for an observation of interface modes.

Increasing the electronic temperature causes a subsequent deterioration of the modulation of the resonance pattern, as is seen in Fig. 12, computed within the dielectric continuum model. This trend is in agreement with the results of the mobility calculations,[4,5] indicating that the modulation of the cooling rate curve should be highest at the low-temperature edge of the range of validity of the present model. The low-$d$ nonresonance maximum, observed at $T=50$ K near $d=75$ Å, subsequently shifts to lower values of $d$ with increasing temperature. As stated above, the position of this maximum is the result of combination of several factors which show the dependence of $r$ on the well width and on $T_e$. The temperature dependence of the low-$d$ part of $r$ can be partly understood when a different plot of the data contained in Fig. 12 is performed. The result is presented in Fig. 13. Here the cooling rate is plotted against the inverse electronic temperature $1/T_e$. The curves obtained are nearly linear. Ignoring the fact that the temperature of the phonon modes is not zero, the curves are fitted to the exponential dependence of the cooling rate[19]

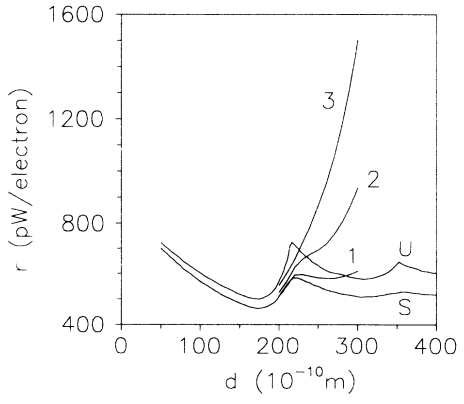


FIG. 11. Power loss per electron, $r$, as a function of the well width, at $T_e=100$ K, $T_L=4.2$ K, and $n_e=10^{22}$ m$^{-3}$. Curve $S$, static screening included; curve $U$, without screening. Curves 1, 2, and 3 are computed with the screening included, at the electric-field intensity $F$ equal to 0.1, 0.2, and 0.3, respectively, in units of $10^7$ V/m.

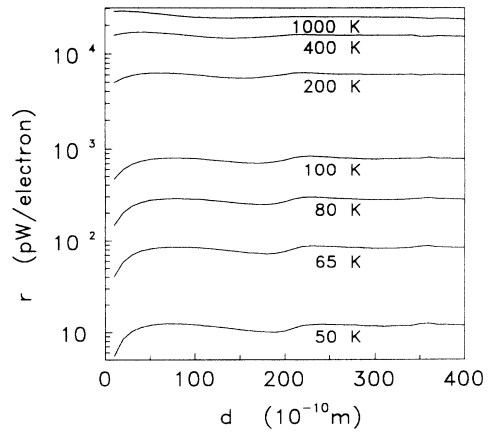


FIG. 12. Dependence of the power loss per electron on electronic temperature $T_e$.

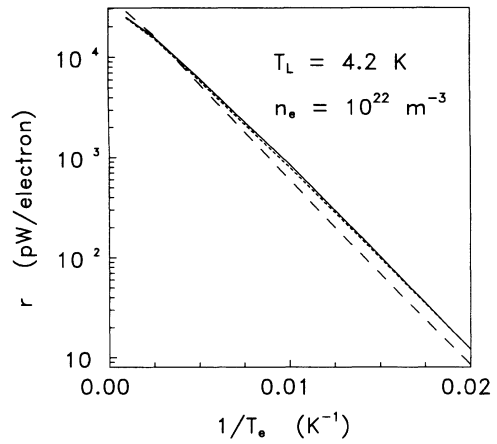


FIG. 13. Semilogarithmic plot of power loss per electron for $d=20$ (dashed), 100 (dotted), and 230 Å (full).

$$r \sim \exp\left[-\frac{\hbar\Omega}{k_B T_e}\right], \tag{49}$$

in which $\Omega$ should correspond to the phonon frequency in the case of a single-phonon frequency model. The fit was performed for the 20-Å curve at $T_e=50$ and 200 K. At the low temperature of 50 K we get $\Omega=5.484\times10^{13}$ $s^{-1}$. This frequency is only slightly larger than the frequencies $\Omega_{S-}(q)$ (see Ref. 31 for a graphical presentation of the $q$ dependence of the interface mode frequencies for the presently considered quantum-well structure with $d=20$ Å). At the higher temperature of $T_e=200$ K the fit gives $\Omega=5.8214\times10^{13}$ $s^{-1}$. This increase of the effective phonon frequency can be ascribed to the influence of the $(S+)$ interface mode coming into play at the increased temperature. The latter frequency of $\Omega=5.8214\times10^{13}$ $s^{-1}$ is found to be roughly in between the frequencies of $(S-)$ and $(S+)$ modes,[31] but it is larger than the confined mode frequency of GaAs. This is why the cooling rate at $d=20$ Å tends to increase faster with increasing temperature than the cooling rate at larger well widths, and why the nonresonant maximum moves toward a lower $d$ with increasing $T_e$.

The other two curves in Fig. 13, corresponding to $d=100$ and 230 Å, are practically indistinguishable. The fit was done for the $d=230$-Å curve at the electronic temperature of 100 K. The frequency $\Omega=5.248\times10^{13}$ $s^{-1}$, obtained by the fitting, is quite close to the frequency of $\omega_{L1}=5.496\times10^{13}$ $s^{-1}$ of the confined GaAs mode expected to determine the temperature dependence of the cooling rate in the case of larger well widths. The difference between the latter fitting frequency of $\Omega=5.248\times10^{13}$ $s^{-1}$ and that of $\omega_{L1}$ can be ascribed to a certain role which is still played by the interface low-frequency mode $(S-)$ at $d=230$ Å. The slight bending of the curves at temperatures of about 400 K can be ascribed to a beginning of an insufficiency of confining the number of the subbands, and of the number of the confined modes, to five only.

The variations of the interface mode frequencies, in that range of the phonon wave vector at which these modes contribute to the hot-electron cooling, is not negligible, so that the fitting of the data to a simple formula like (49) does not allow for a detailed insight into the role of the individual interface modes. Nevertheless, although the positions of the resonance maxima in the hot-electron cooling rate resonance pattern are not likely to allow easy distinguishing between the confined and interface modes, the variation with the electronic temperature of the slope of the logarithmic plot of the cooling rate against $1/T_e$, in narrow wells, should allow us to demonstrate the participation of the interface-phonon branches on the hot-electron cooling rate in narrow wells.

## V. CONCLUSIONS

The electrophonon resonance in the $Al_xGa_{1-x}As$-GaAs Q2D quantum wells has been studied for the long-wavelength optical-phonon generation and for the hot-electron cooling rate. As parameters controlling the onset of the electrophonon resonance, the quantum-well width and the electric field normal to the interfaces have been considered. The effect has been studied in quantum wells having a square-shaped potential profile, using two models of the optical lattice vibrations, namely the bulk-phonon model and the dielectric continuum model.

It has been found that the long-wavelength optical-phonon generation rate gives a resonance pattern with a very distinct modulation for both the quantum-well width and the electric-field control of the onset of the resonance. The very strong modulation of the resonance pattern concerns both the confined, or bulk, phonons and the interface phonons. The intensity of the resonance maxima of the LW generation rate for the interface modes is found to be comparable to that of the confined modes, in the range of 200–400 Å of the well width.

The modulation of the hot-electron cooling rate resonance pattern is found to be less pronounced than that of the LW-phonon generation, for both the well width and electric-field control of the resonance. In particular the hot-electron cooling rate electrophonon resonance is not likely to allow for easy distinguishing between confined and interface modes, although the temperature dependence of the hot-electron cooling rate in the narrow wells appears to provide a possibility of observing the difference between the energies of the confined and interface modes of the lattice vibrations.

The comparison of the two presently considered versions of the electrophonon resonance seems to indicate that an electrophonon resonance based on a quantity which is integral with respect to the optical-phonon generation rate is less pronounced because of a relatively high contribution of the signal, which comes from the processes of a nonresonant nature. On the other hand, the resonance signal of the LW-phonon generation rate appears to be more directly related to the phenomenon of the resonance intersubband optical-phonon scattering.

## ACKNOWLEDGMENTS

This work has been supported by National Science Council of Taiwan, by Grant Nos. NSC 82-0208-M-006-057 and NSC-83-0102-C006-003-SM.

*On leave from Institute of Physics, Academy of Sciences of Czech Republic, Prague, Czech Republic.

[1]P. Kocevar, in *Progress on Electron Properties of Solids,* edited by R. Girlanda *et al.* (Kluwer Academic, Dordrecht, 1989), pp. 125–138.

[2]M. C. Tatham and J. F. Ryan, Semicond. Sci. Technol. **7**, B102 (1992).

[3]S. Briggs and J. P. Leburton, Superlatt. Microstruct. **5**, 145 (1989).

[4]F. M. Peeters and J. T. Devreese, Semicond. Sci. Technol. **7**, B15 (1992).

[5]W. Xu, F. M. Peeters, and J. T. Devreese, Phys. Rev. B **48**, 1562 (1993).

[6]K. Král, Z. Khás, and B. Hejda, Phys. Status Solidi B **176**, K25 (1993).

[7]M. C. Tatham and J. F. Ryan, Semicond. Sci. Technol. **7**, B102 (1992).

[8]K. T. Tsen, R. P. Joshi, D. K. Ferry, and H. Morkoç, Phys. Rev. B **39**, 1446 (1989).

[9]Tobias Ruf, Keith Wald, Peter Y. Yu, K. T. Tsen, H. Morkoç, and K. T. Chan, Superlatt. Microstruct. **13**, 203 (1993).

[10]J. Motohisa and H. Sakaki, Appl. Phys. Lett. **60**, 1315 (1992).

[11]B. Hejda and K. Král, Phys. Rev. B **47**, 15 554 (1993).

[12]K. Král and B. Hejda, Phys. Rev. B **48**, 11 461 (1993).

[13]K. Král, Z. Khás, and B. Hejda, Phys. Status Solidi B **148**, K129 (1988).

[14]K. Král, Phys. Status Solidi B **170**, 537 (1992).

[15]K. Král, B. Hejda, and Z. Khás, Key Eng. Mater. **65**, 215 (1992).

[16]L. Wendler, Phys. Status Solidi B **129**, 513 (1985).

[17]M. V. Klein, IEEE J. Quantum Electron. **QE-22**, 1760 (1986).

[18]A. K. Sood, J. Menendez, M. Cardona, and K. Ploog, Phys. Rev. Lett. **54**, 2115 (1985).

[19]S. Das Sarma, V. B. Campos, M. A. Stroscio, and K. W. Kim, Semicond. Sci. Technol. **7**, B60 (1992).

[20]X. F. Wang and X. L. Lei, Phys. Rev. B **49**, 4780 (1994).

[21]Mao-long Ke and B. Hamilton, Phys. Rev. B **47**, 4790 (1993).

[22]B. Danilchenko, S. Roshko, M. Asche, R. Hey, M. Höricke, and H. Kostial, J. Phys. Condens. Matter **5**, 3169 (1993).

[23]J. Callaway, *Quantum Theory of the Solid State, Part B* (Academic, New York, 1974).

[24]P. J. Price, Surf. Sci. **113**, 199 (1982).

[25]P. Price, J. Vac. Sci. Technol. **19**, 599 (1981).

[26]H. Sato, Jpn. J. Appl. Phys. **21**, 1181 (1982).

[27]C. Guillemot and F. Clérot, Phys. Rev. B **44**, 6249 (1991).

[28]K. Huang and B. Zhu, Phys. Rev. B **38**, 13 377 (1988).

[29]R. Fuchs and K. L. Kliever, Phys. Rev. **140**, A2076 (1965).

[30]J. J. Licari and R. Evrard, Phys. Rev. B **15**, 2254 (1977).

[31]L. Wendler and R. Pechstedt, Phys. Status Solidi B **141**, 129 (1987).

[32]M. Babiker, J. Phys. C **19**, 683 (1986).

[33]L. P. Kadanoff and G. Baym, *Quantum Statistical Mechanics* (Benjamin, New York, 1962).

[34]P. Lipavský, V. Špička, and B. Velický, Phys. Rev. B **34**, 6933 (1986).

[35]D. N. Zubarev, *Neravnovesnaya Statisticheskaya Termodinamika* (Nauka, Moskva, 1971).

[36]N. N. Bogolyubov and N. N. Bogolyubov, Jr., *Vvedenye v Kvantovuyu Statisticheskuyu Mekhaniku* (Nauka, Moscow, 1984).

[37]W. Cai, M. C. Marchetti, and M. Lax, Phys. Rev. B **34**, 8573 (1986).

[38]M. C. Marchetti, W. Cai, and M. Lax, Solid State Electron. **31**, 677 (1988).

[39]S. Peletminskii and A. Yatsenko, Zh. Exp. Teor. Fiz. **53**, 1327 (1967) [Sov. Phys. JETP **26**, 773 (1968)].

[40]T. Kawamura, S. Das Sarma, R. Jalabert, and J. K. Jain, Phys. Rev. B **42**, 5407 (1990).

[41]L. Reggiani, in *Hot Electron Transport in Semiconductors,* edited by L. Regiani, Topics in Applied Physics Vol. 58 (Springer-Verlag, Berlin, 1985).

[42]*Zahlenwerte and Funktionen aus Naturwissenschaft und Technik,* edited by K.-H. Hellwege, Landolt-Börnstein, New Series, Vol. 17, Pt. a (Springer-Verlag, Berlin, 1982).

[43]S. Adachi, J. Appl. Phys. **58**, R1 (1985).

[44]L. I. Schiff, *Quantum Mechanics* (McGraw-Hill, New York, 1971).

[45]X. F. Wang and X. L. Lei, Phys. Rev. B **47**, 16 612 (1993).